Fundamental studies of ultrasonic melt processing

D.G. Eskin[1,5], I. Tzanakis[2], F. Wang[1], G.S.B. Lebon[1], T. Subroto[1], K. Pericleous[3], J. Mi[4]

[1] BCAST, Brunel University London, Uxbridge UB8 3PH, UK

[2] MEMS, Oxford Brookes University, MEMS, Oxford, OX33 1HX, UK

[3] CSEG, University of Greenwich, SE10 9LS, UK

[4] School of Engineering & Computer Science, University of Hull, Hull, HU6 7RX, UK

[5] Tomsk State University, Tomsk, 634050, Russian Federation,

Abstract

Ultrasonic (cavitation) melt processing attracts considerable interest from both academic and industrial communities as a promising route to provide clean, environment friendly and energy efficient solutions for some of the core issues of the metal casting industry, such as improving melt quality and providing structure refinement. In the last 5 years, the authors undertook an extensive research programme into fundamental mechanisms of cavitation melt processing using state-of-the-art and unique facilities and methodologies. This overview summarises the recent results on the evaluation of acoustic pressure and melt flows in the treated melt, direct observations and quantitative analysis of cavitation in liquid aluminium alloys, in-situ and ex-situ studies of the nucleation, growth and fragmentation of intermetallics, and de-agglomeration of particles. These results provide valuable new insights and knowledge that are essential for upscaling ultrasonic melt processing to industrial level.

Keywords: aluminium; in situ characterisation; acoustic pressure; acoustic streaming; ultrasonic melt processing; structure refinement; heterogeneous nucleation; fragmentation; de-agglomeration .

1. Introduction

Ultrasonic melt processing (USP) has been proven on the industrial scale to be an effective method for degassing, filtration, and grain refinement of aluminium and

magnesium alloys [1, 2, 3, 4]. In the past, the challenge of treating large melt volumes was met by using multiple ultrasonic sources [1, 2]. This complex and energy-demanding approach works well in batch degassing operations in foundries or for grain refining or degassing a single cast billet/ingot in direct-chill casting. However, when it comes to casting multiple strands of extrusion billets, it becomes too technologically complicated and expensive. In addition, the introduction of other competitive techniques in industry in the 1980s (e.g. Ar-rotary degassing and Al5Ti1B grain refiner), has stalled the uptake of USP. Interest in USP was recently revived due to its attractive advantages such as environmental friendliness and energy efficiency. Current research concentrates on achieving high efficiency in processing large melt volumes by using a single (or limited number of) ultrasonic radiator with a well-designed flow arrangement. The success of such operation requires in-depth knowledge of the underlying physical mechanisms of USP, supported by adequate and validated numerical modelling.

In the past the USP was studied either by *in-situ* observations in transparent liquids or by correlation of ultrasonic parameters to *post-mortem* observations of as-cast alloy structure. The main phenomena and mechanisms established can be briefly described as follows:

High-frequency oscillations of an ultrasonic source (sonotrode) (typically in the range above 16-17 kHz) result in the formation of cavitation bubbles (typically on “cavitation nuclei” represented either by gas bubbles or inclusions) and in acoustic streaming in the processed liquids [3, 5]. Reports on direct observations of cavitation and acoustic streaming are limited and most of those are done in transparent low temperature liquids. Cavitation bubbles nucleate in a region below the sonotrode that is called the “cavitation zone”. To initiate cavitation, a certain pressure in the liquid phase, termed “cavitation threshold”, needs to be overcome. The required pressure can be calculated theoretically or determined experimentally using hydrophones or cavitometers [5]. In real liquids, including metallic melts, the actual cavitation threshold is lower than the theoretical threshold due to the presence of the cavitation nuclei. With increasing ultrasonic frequency, liquid viscosity, and surface tension, the cavitation threshold increases [6]. The acoustic pressure decreases exponentially with distance from the source, an effect that is called “attenuation”; this effect has been predicted by modelling. As the cavitation develops, a significant portion of acoustic energy is consumed in the cavitation zone. Due to the very large number of cavitation

bubbles, the cavitation zone becomes a low-density region with high volume occupied by gas/vapour. As a result, the cavitation zone “shields” the bulk of the volume from the ultrasonic waves and the attenuation becomes even more pronounced [5]. Acoustic pressue and flow measurements in liquid metals have been rather rudimentary and qualitative so far, with cavitation intensity (level of white noise from imploding cavitation bubbles) being the most widely used parameter for cavitation activity.

The theory of ultrasonic degassing has been developed in the 1970s for water with some measurements of oxygen concentration [7] and then applied to aluminium melts based on hydrogen measurements in as-cast alloys [1, 2]. Analytical modelling established the main principles of rectified diffusion of dissolved gas into an oscillating bubble, its growth, and flotation.

One of the main applications of USP is related to microstructure refinement. There are a number of suggested mechanisms for this effect, most of which are based on theoretical estimates with indirect experimental evidence. In particular, heterogeneous nucleation during solidification is assumed to be related to the so-called “activation of inclusions” [2, 4]. The activation can be a result of improved wetting of inclusions (e.g. oxides in liquid aluminium), which is also related to a sonocapillary effect [2, 8, 9]. Although the sonocapillary effect has been observed experimentally on the macroscopic scale, it has never been confirmed for the case of microscopic inclusions in liquid metals. There is very limited and indirect evidence of the nucleation of intermetallics and matrix crystals on oxides, including the facilitation of this process by ultrasonic cavitation [2].

Another mechanism of structure refinement is fragmentation of growing crystals by ultrasonic cavitation. There are some direct observations of crystal fragmentation by cavitation bubbles in transparent analogues and with limited resolution [1, 10]. No thorough analysis of the fragmentation mechanisms has been performed yet. The role of acoustic streaming in this process is reserved only for the distribution of fragments in the bulk liquid.

The modelling description of USP is very limited due to the numerical difficulties of addressing multi-scale and multi-physics phenomena, although the physics of single bubble oscillation and implosion are rather well known and numerically/analytically described. Realistic simulations of cavitation phenomena are also difficult due to the nonlinearity of the problem [11]. Recent attempts of cavitation modelling in water include models that couple the evolution of cavitation and acoustic fields by solving a nonlinear Helmholtz equation that

accounts for bubble dynamics [12, 13, 14]. This nonlinear model can be used to predict acoustic streaming in the presence of cavitation [15].

In the last decade, a wealth of new knowledge on USP has been generated, to a great extent, due to the availability of new analytical and characterisation techniques (*in situ* synchrotron imaging and high-speed filming, acoustic measurements, particle-image velocimetry) and modelling approaches.

In this paper, we give an overview of our research in the last 5 years. The paper highlights the important phenomena in USP and illustrates those with our own results. For more detailed information on relevant experimental and modelling procedures and results, the reader is referred to the original papers.

2. Acoustic measurements

USP is inherently related to the propagation of acoustic waves in the liquid, succession of negative and positive acoustic pressure cycles, and acoustic cavitation. The measurement of acoustic spectra and pressure in a liquid is often made by using hydrophones in low-temperature liquids. Direct measurements in liquid metals (including aluminium) were only recently made possible due to the development and calibration of a high-temperature cavitometer [16]. Originally designed for qualitative measurements of acoustic noise and cavitation intensity, this cavitometer was calibrated in the National Physical Laboratory (NPL, UK) and applied to acquire accurate acoustic spectra and measure acoustic pressure in a wide range of frequencies (from 15 kHz up to 10 MHz).

It became, therefore, possible to quantify for the first time the distribution of acoustic pressure in the treated melt volume, and better understand the attenuation of acoustic waves in the melt. In the series of experiments presented here, we used a 1-kW piezoelectric transducer coupled with a ceramic sonotrode at a driving frequency of 20 kHz. A charge of 2 l (5.2 kg of commercially pure liquid Al or 2 kg of water) was held inside a clay-graphite glazed crucible 150 mm in diameter and 180 cm deep. The liquid height was 120 mm. The sonotrode was submerged 10 mm below the liquid surface in the middle of the crucible. The measurements were made with a cavitometer placed 70 mm below the liquid surface in three positions: under the sonotrode, at half-radius of the crucible, and close to the crucible wall. The temperature changed from 26 °C to 49 °C in water (due to the introduction of

acoustic energy; however, repeated checks showed no effect of this change on the measured results in these series of experiments) and maintained at 703±3 °C in aluminium. The power of the transducer was varied; and the transmitted acoustic power and the corresponding maximum acoustic pressures under the sonotrode are listed in Table 1. Examples of measured acoustic emissions and pressure in water and liquid aluminium are shown in Fig. 1. These studies led to the following new findings: (a) the highest ultrasonic power is not necessarily the best one for treating larger volumes (Fig. 1c); (b) sound waves attenuate much stronger with distance and more uniformly with regard to the acoustic power in water (80% attenuation, Fig. 1b) than in liquid aluminium (30-50%, Fig. 1c), which may reflect more developed cavitation in water due to abundance of vapour bubbles and, hence, more substantial shielding of acoustic waves by the cavitation zone; and (c) acoustic pressures are significantly higher in liquid Al than in water [17, 18].

Table 1. Transmitted acoustic power and measured maximum acoustic pressure in water and liquid aluminium.

Power on the transducer, %	Transmitted power into the treated water, W	Maximum acoustic power in water, MPa	Transmitted power into the treated aluminium, W	Maximum acoustic power in aluminium, MPa
50	210	2.53±0.09	228	15.4±1.9
60	250	2.65±0.04	276	15.1±1.4
70	305	2.72±0.08	343	14.1±1.5
80	385	2.63±0.07	456	13.5±1.5
90	480	2.69±0.08	522	11.3±1.2
100	550	2.78±0.07	538	9.4±1.7

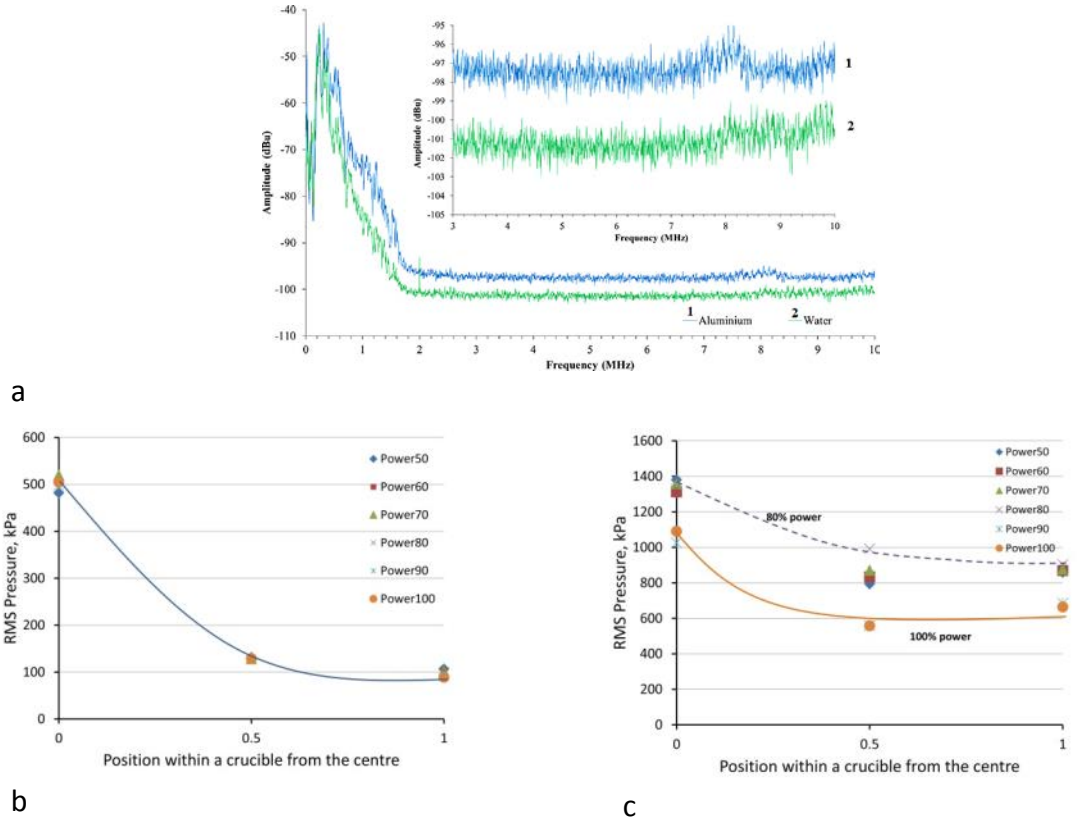

Figure 1: Experimental measurements of acoustic emissions and pressure: (a) acoustic spectra acquired under the sonotrode in water (lower curve and liquid aluminium (upper curve) and distribution of average acoustic pressure with a distance from the sonotrode in the same volume (2 l) of water (b) and liquid aluminium (c). See Table 1 for the acoustic power in W corresponding to the transducer power in %.

The acoustic pressure measured in most liquid at the driving frequency under cavitation conditions is several times lower than theoretical values in the absence cavitation. This is a direct result of the shielding effect. In water, root mean square (RMS) acoustic pressures at 1 MHz in the acquired acoustic spectrum (associated with acoustic emissions from the collapse of cavitating bubbles) were found to be 2–3 times lower than in liquid aluminium [17], indicating that the potential energy is stored in relatively long living Al cavitation bubbles as shown in [19] and then released back into the bulk in a form of collapsing events.

The results shown in Fig. 1c confirm that cavitation treatment in liquid aluminium can be performed at some distance/volume around the cavitation zone. A lower acoustic power (at least in liquid aluminium) maybe beneficial due to a lesser shielding effect and a wider

propagation of powerful acoustic waves outside the cavitation zone. Acoustic pressures in liquid aluminium are certainly high enough to break clusters of particles and facilitate the de-agglomeration process and wetting through the sono-capillary effect [4, 20].

Systematic measurements of cavitation spectra and pressure in bulk volume of liquid aluminium [21] demonstrated that, the most important USP parameter that determines the intensity of acoustic cavitation is the distance from the sonotrode. Melt temperature also affects cavitation albeit to lower extent: the lower the temperature, the stronger the cavitation. The source acoustic power has an ambivalent influence: more cavitation is expected with higher powers, but the shielding effect of the developed cavitation zone may increase attenuation, thereby limiting the affected liquid volume. It was also experimentally shown that physical properties of the treated liquid may significantly change the appearance, dynamics and extent of cavitation [18]. For example, the cavitation region in high-viscosity glycerine is very well defined and confined in volume with very strong (though slow) acoustic streaming and recirculation. Cavitation bubbles are formed only close to the sonotrode surface. In a low-density and low-viscosity ethanol, the cavitation development occurs in a larger volume without any stable or well defined cavitation zone and acoustic streaming pattern. The cavitation bubbles are, however, rather stable over the considerable liquid volume, slowly expanding before floating to the liquid surface. The experiments also confirmed that water qualitatively resembled liquid aluminium in cavitation development, exhibiting very similar cavitation behaviour as compared to other tested liquids: hence, water can be used as a transparent analogue for aluminium (except for the attenuation phenomenon).

Acoustic measurements were also applied in testing a new scheme of ultrasonic degassing with a plate sonotrode. It was confirmed that this novel design of a sonotrode indeed generated acoustic cavitation with the formation of large stable bubbles suitable for degassing [22]. The new sonotrode design allowed for 25–30% increase in degassing efficiency as compared with a traditional cylindrical sonotrode due to the multiple locations of cavitation excitation along the length of a plate vibrating in a flexural mode [22].

In an attempt to understand the fundamentals of USP, an acoustic cavitation model was developed to predict the evolution of the bubble cloud structure and acoustic pressure inside a sonicated liquid. Based on the nonlinear bubbly equations proposed by van Wijngaarden [23] and mathematically derived by Caflisch *et al.* [24] using Foldy's method

[25], the model couples the wave equation (governing sound propagation in a moving fluid) and the Rayleigh–Plesset equation (for bubble dynamics). To minimise the effects of numerical dispersion, the wave equation is discretized in space using a 6-point stencil and in time using a 4-point stencil. For stability, the bubble dynamics equation is solved using a multi-stage explicit solver. Figure 2 demonstrates the modelling results for USP of aluminium at 17.7 kHz in a crucible, assuming a bubble density of 1×10^{11} m^{-3} and initial radii of 1 µm. The pressure-distance relationship obeys a power law, and the attenuation of pressure with distance agrees well with experimental results [21]. Such a macroscopic model is essential for the optimization of USP in scaled-up application, e.g. ultrasonic degassing in a ladle/launder or grain refinement upon direct-chill casting.

In parallel, a theoretical study of the interaction of hydrogen bubbles in liquid aluminium was undertaken to understand the interplay between bubble resonance and degassing [26]. By adapting the equations derived by Doinikov [27] to aluminium, it was found that large forcing signals in the order of MPa were required for fast degassing, especially when the frequency of the forcing signal is less than 22 kHz (favourable frequencies for degassing aluminium melt).

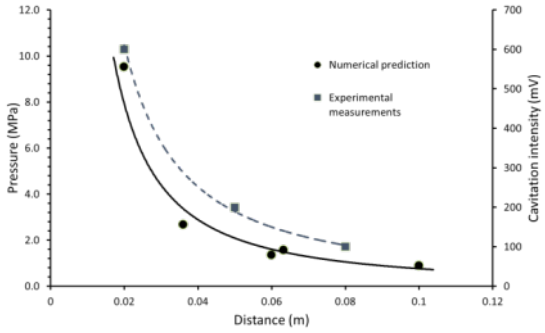

Figure 2: Variation of maximum pressure with distance from sonotrode [28] and comparison with experimental cavitation intensity [21].

3. In-situ studies

3.1 Synchrotron observations of cavitation

The development of state-of-the-art synchrotron X-ray facilities, as well as image acquisition capability and processing software, made it possible to study the dynamics of ultrasonic processing of liquid and solidifying metals [29, 30], e.g. observingin-situ the implosion and oscillation of ultrasonic bubbles [31], as well as size distribution of cavitation

bubbles in relation to the acoustic power and frequency; their interaction with intermetallics, solid particles and solidification front; acoustic flows; and sono-capillary effect.

Figure 3a shows a bubble oscillation and implosion in a liquid Bi–8% Zn alloy (427 °C, an ultrasound power of 20 W) taken using the ultrafast (up to 271,554 fps) synchrotron X-ray imaging at 32-ID-B of Advanced Photon Source. Bubble implosion occurred immediately below the sonotrode under an ultrasonic intensity of 276 W/mm^2. Figure 3b shows the bubble radius measured from the images, and their correlation to the acoustic pressure applied into the liquid metal. The dashed lines indicate the sudden drop of bubble radius at the instance of bubble implosion [31].

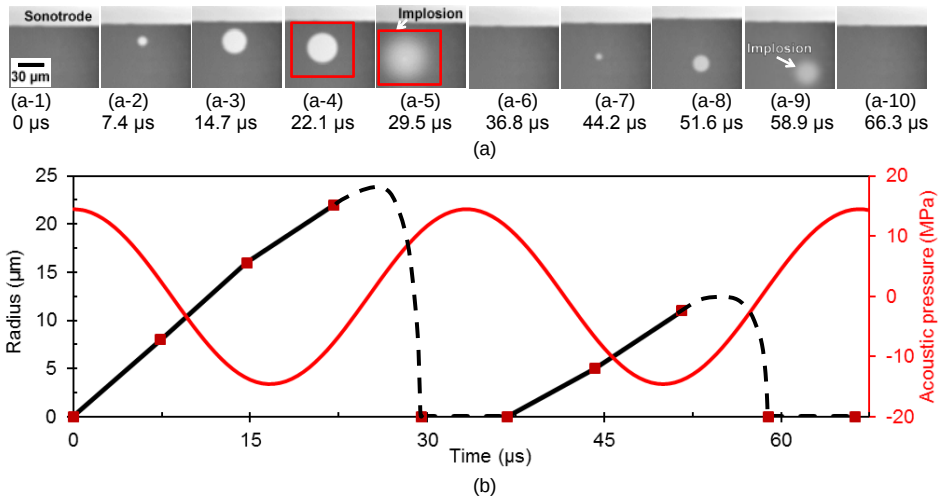

Figure 3: (a) An X-ray image sequence acquired using 135,780 fps at Sector 32-ID-B of APS, showing the bubble implosion immediately below the sonotrode tip in a Bi–8% Zn alloy. (b) The bubble radius evolution and correlation with the acoustic pressure applied into the liquid metal (adapted from [31]).

Figure 4 shows selected images of a transient bubble (framed) in a liquid Al–10% Cu alloy taken in by synchrotron X-rays. The size of this bubble is in good agreement with the Minnaert equation [32] that gives 70 μm for the bubble resonance radius at the 30 kHz driving frequency.

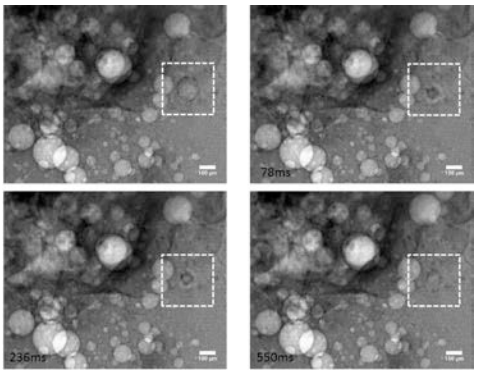

Figure 4: The transient behaviour of a cavitation bubble in an Al–10 wt% Cu melt (640 °C, 30 kHz, 800 W/cm^2) captured by synchrotron X-rays.

A statistical size distribution of stable cavitation bubbles observed in similar experiments and their growth kinetics are illustrated in Fig. 5.

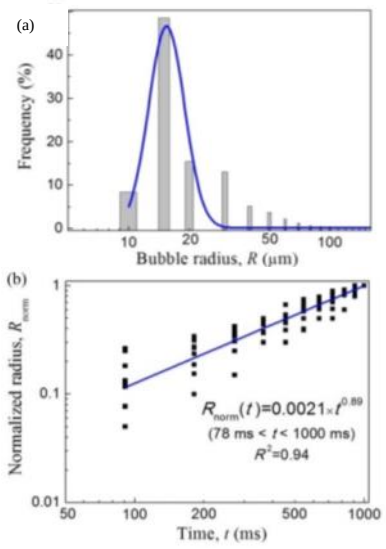

Figure 5: Experimentally measured bubble size distribution (a) and growth kinetics (b) of stable cavitation bubbles in an Al-10 wt% Cu melt (640 °C, 30 kHz, 800 W/cm^2) (after [19]).

Macroscopic acoustic streaming originated from the cavitation zone can be also captured in liquid metals using synchrotron X-ray imaging. An example shown in Fig. 6 gives a typical flow pattern with a downstream flow and two recirculation vortices on either side. There is a clear similarity with the acoustic streaming observed in water and glycerine (see Fig. 8 below). As this image was taken during solidification of a Sn-Cu alloy, the fragmented dendrites drawn into the melt bulk by the acoustic flow are also visible as (shown by

arrows). This observation clearly confirms one of the grain refinement mechanisms of USP, i.e. fragmentation and dispersion of solid phase by cavitation and acoustic streaming.

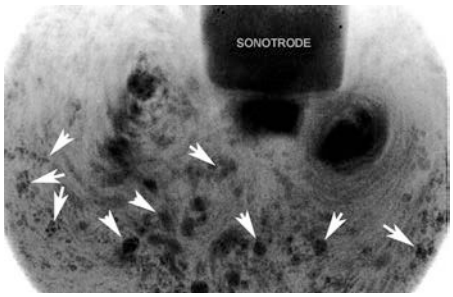

Figure 6: Acoustic streaming and dendrite fragmentation (arrows) observed in a synchrotron using a Sn–30 wt% Cu alloy and 100 W acoustic power.

One of the current applications of USP is the introduction of nanoparticles in liquid aluminium or magnesium, with the aim of manufacturing nanocomposite materials [33, 34]. USP is used to improve wetting of nanoparticles, de-agglomerate their conglomerates, and improve the dispersion of nanoparticles. Synchrotron X-ray studies allowed, for the first time, the observation and quantification of the sonocapillary effect that is responsible for de-agglomeration, improved filtration and wetting (and possibly for the activation of inclusions) [20, 35]. These studies also demonstrated that the presence of nanoparticles in the melt significantly intensified acoustic flows and cavitation as demonstrated in Fig. 7 [36].

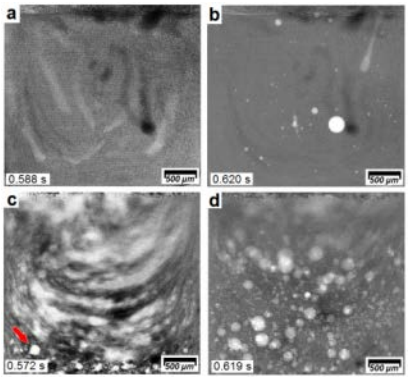

Figure 7: Synchrotron X-ray observation of flow patterns and cavitation bubble population in an Al–10 wt% Cu alloys (a, b) and an Al–10 wt% Cu alloy with 0.05 wt% of 80-nm Al_2O_3 particles (c, d) (700 °C, 30 kHz, 800 W/cm^2) [36]. (a, c)–during USP, (b, d)–immediately after USP has been stopped.

3.2 Study of cavitation in transparent liquids

Despite recent advances in synchrotron studies of liquid metals, transparent media are still widely used for *in situ* observations, allowing for more detail to be captured. Water is proven to be similar to liquid aluminium in ultrasonic cavitation development and is frequently used as a transparent alternative in USP studies. The study of cavitation processing also goes beyond liquid metal applications and is relevant to other USP areas such as food, chemical, drug, and fuel manufacturing where transparent liquids of different properties can be used.

We have studied the cavitation development in three liquids with significant differences in viscosity, vapour pressure, surface tension, and density. These parameters are key factors that determine cavitation behaviour [4]. This research demonstrated vast differences in cavitation kinetics, dynamics, macroscopic patterns, as well as in associated acoustic spectra.

Figure 8 illustrates the geometry and kinetics of development for cavitation zones and acoustic streaming patterns in de-ionised water, glycerine, and ethanol.

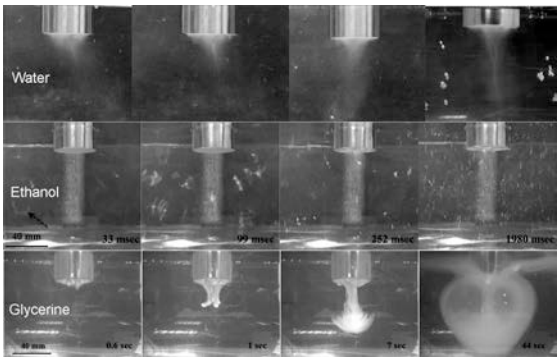

Figure 8: The development of the cavitation zone and acoustic flow patterns in three transparent liquids: water (upper row), ethanol (middle row) and glycerine (lower row) (RT, 20 kHz, acoustic power 90, 78 and 230 W at the same oscillation amplitude 17 µm p-p) (after [18]).

The active cavitation zone outline is clearly observed in water (conical bubble structure) and in glycerine (thick round layer), while in ethanol the cavitation bubbles are dispersed and vigorously oscillate towards the free surface (similar to liquid degassing) rather than creating complicated bubbly structures and multiple collapsing events.

Acoustic measurements [18] reveal that the cavitation intensity (measured in dBu) are similar in water and glycerine but considerably lower in ethanol. On the other hand, bubbles in ethanol survive longer, thus giving rise to distinctive pressure peaks at MHz frequencies. It is also demonstrated that water shows the closest cavitation behaviour to liquid aluminium, as indicated by the spectra analysis and selected dimensionless quantities; and can therefore be used as a transparent analogue of liquid Al. There is, however, a potential to design transparent liquids closer matching properties to liquid metals using cavitometer measurements.

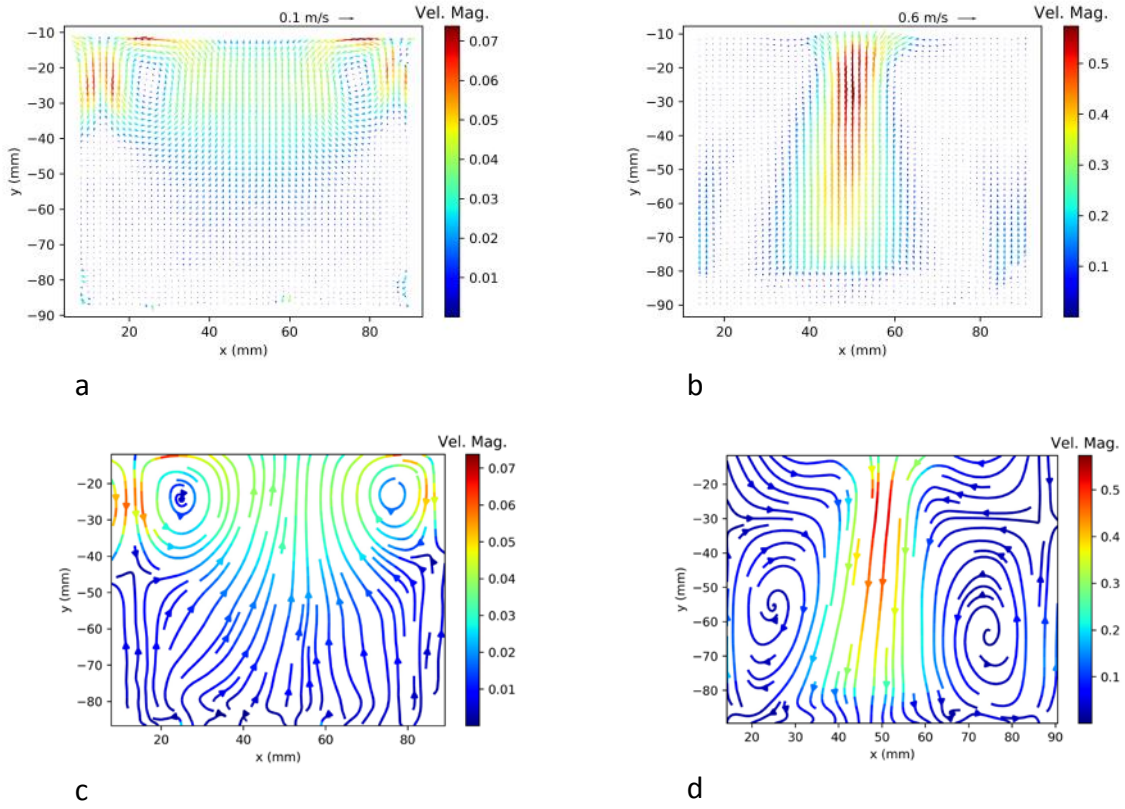

Figure 9: Typical average velocity fields (a, b) and stream lines (c, d) measured with PIV below the sonotrode tip at a low (a, c) and high (b, d) transducer power settings. The axial direction of streaming is upwards in (a, c) and downwards in (b, d). Legend: velocity magnitude in m/s (0.01–0.1 left, 0.04–0.6 right).

Acoustic streaming in transparent liquids can be successfully studied using particle-image velocimetry (PIV) [37]. Recently, we have established an interesting acoustic flow pattern in water at lower acoustic powers using a 20 kHz transducer coupled with a titanium sonotrode of 20 mm in diameter submerged 2 cm below liquid surface. The dominant axial

flow direction is upwards towards the centre of the sonotrode tip (24 µm p–p amplitude; 50% power; 20 kHz) with the average flow velocity 0.03-0.1 m/s (Fig. 9a). At a higher power (51 µm p–p amplitude; 100% power, 20 kHz), a downward jet with an average velocity of 0.1-0.5 m/s (Fig. 9b) is observed. Interestingly, in the case of the lower power, dominant vortices with velocities up to 0.09 m/sec (comparable on the same scale to the centreline stream) are formed near the cavitation zone maximising the effect of recurculating and processing of floating phases (Fig. 9c), in contrast to the higher power, where vortices significantly weaker than the downstream centreline jet are formed further away from the tip of the sonotrode (Fig. 9d). Numerical analysis may shed light to this interesting mechanism and possibly reveal the nature of this inverse flow. Some preliminary computer simulations indicate that this phenomenon is related to the intensity of cavitation, i.e. the number density and size of cavitation bubbles in the cavitation zone.

4. Mechanisms of structure refinement

4.1 Enhanced heterogeneous nucleation

Refinement of primary grains and intermetallics by USP is one of the major practical applications. The two main mechanisms are usually considered: cavitation-enhanced heterogeneous nucleation and fragmentation [4]. The role of insoluble inclusions in heterogeneous nucleation assisted by ultrasonic cavitation was considered already in the 1970s [38] and the mechanisms of inclusion activation were developed for aluminium alloys in the 1980s [2]. At this time, however, the hypotheses were based on indirect evidence and some theoretical considerations. Only recently the direct proof of heterogeneous nucleation of primary phases on oxide particles has been obtained [39].

We studied the formation of intermetallic particles Al_3Zr and Al_3Ti during USP above their liquidus and found out that the primary particles were refined [40, 41], Fig. 10 a, b. In almost all cases, a particle was found in the centre of a primary crystal as shown in Fig. 10c. Thorough studies using dissolution of the aluminium matrix, focused ion beam cutting of the crystals, electron diffraction and energy-dispersive X-ray spectroscopy with transmission electron microscopy unambiguously demonstrated that the nucleation of the intermetallics occurred on alumina inclusions with well-defined orientation relationships. The significantly increased amount of primary particles after USP testified for the improved nucleating ability of the indigenous alumina inclusions caused by ultrasonic cavitation.

These results are obtained by *post-mortem* analysis of the structure. It would be, however, very useful to observe the phenomenon of nucleation on oxide particles as it happens, i.e. *in situ*. This was achieved by observation of solidification of an Al-35% Cu alloy with the Al_2Cu phase as a primary intermetallic [39]. In this experiment, the molten alloy has been treated with ultrasonic cavitation and broken pieces of a surface oxide film were entrained into the melt. After the end of USP, the melt was allowed to cool down and the primary Al_2Cu particles started to nucleate and form on the fragments of alumina film (multiple particles as the film is polycrystalline) as shown in Fig. 11. This, to the best of our knowledge, is the first direct evidence of the long-debated issue of nucleation on oxides facilitated by ultrasonic processing.

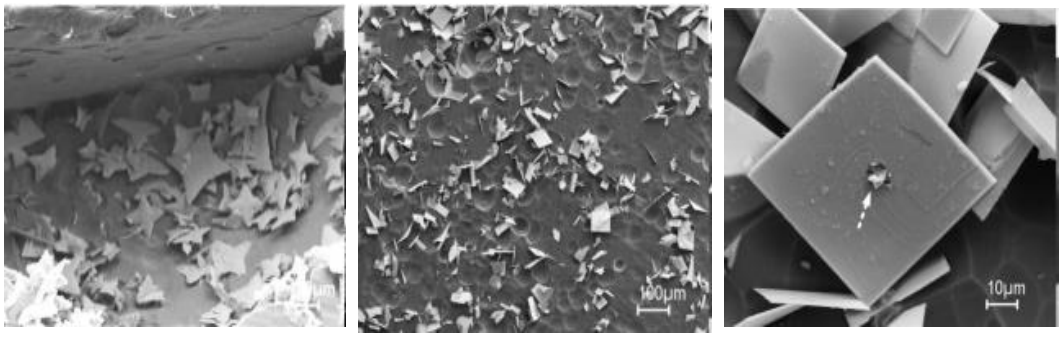

a b c

Figure 10: Refinement of primary Al_3Zr particles in an Al–0.4 wt% Zr alloy: (a) without USP; (b) after USP performed above the liquidus of Al_3Zr and (c) nucleating oxide inclusion inside an Al_3Zr particle.

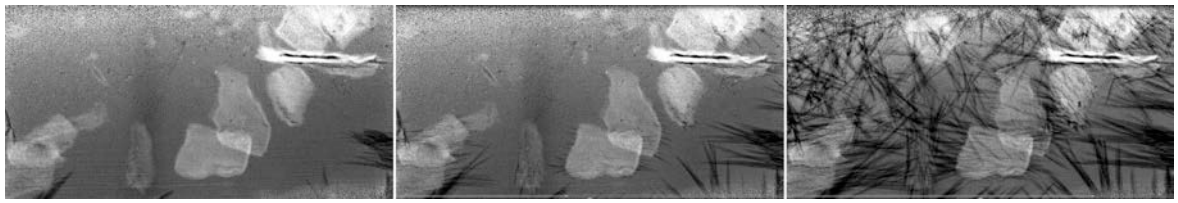

Figure 11: In-situ synchrotron observation of the nucleation of primary Al_2Cu crystals (dark) on the fragments of alumina film (bright) in an Al-35 wt% Cu alloy. Temperature decreases from left to right.

Practical implementation of this mechanism can be found in recent works on oxide-containing master alloys [42, 43]. It was demonstrated that *in situ* formed alumina or spinel particles have good potency for nucleating primary aluminium with a synergetic effect of

USP that enhances the grain refining effect. Figure 12 illustrates this for alumina- and spinel-containing master alloys added to aluminium alloys. The application of USP boosts the nucleating ability of oxides and results in additional grain refining. This is due to two effects: (i) improved wettability of oxide particles and (ii) dispersion of their agglomerates.

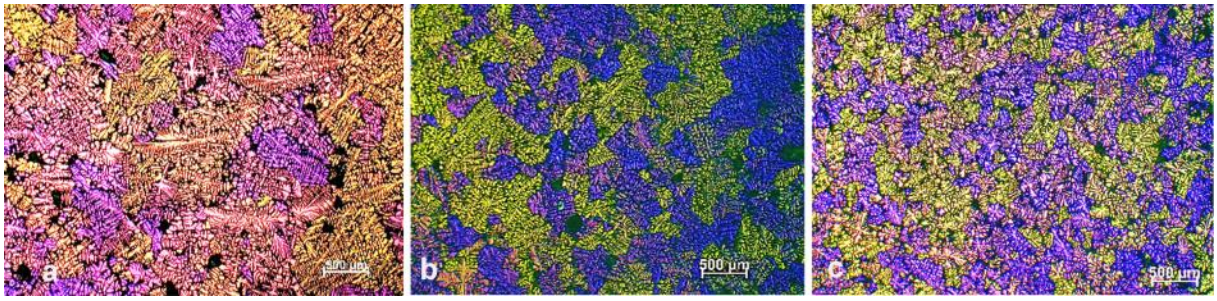

a b c

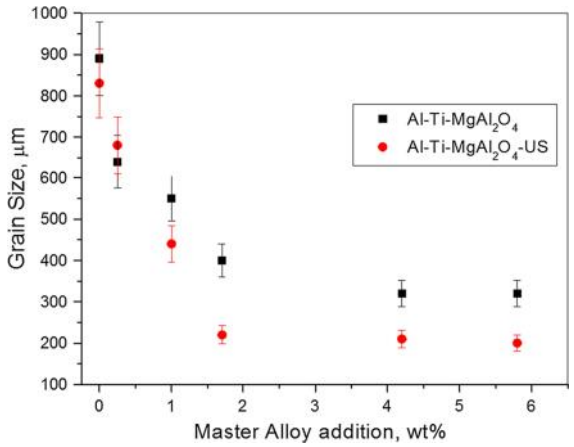

d

Figure 12: Effect of oxides and USP on the grain refining in an A357 (Al-Si-Mg) aluminium alloy: a, A357 cast with USP, no grain refiner; b, A357 cast with an addition of 1% alumina-containing master alloy; c, same as (b) but with USP; d, effects of spinel-containing master alloy addition and USP on the grain size in an A357 alloy.

4.2 Fragmentation of primary crystals

As has been already mentioned, another powerful mechanism of structure refinement upon USP is fragmentation of the solid phase crystals. This mechanism works while the ultrasonic processing is applied in the solidification range of the phase of interest, i.e. below the liquidus. On many occasions, it was shown that fragmentation of primary dendrites of the matrix phase (e.g. Al or Mg), although quite impressive, is confined to a relatively small volume of the treated solidifying alloy, limited by the rapid attenuation of acoustic power

and very restricted acoustic streaming in the presence of the solid phase. There are two practically important cases when this mechanism can work on a larger scale, i.e. direct-chill casting of light alloys [2] and arc-remelting of a vibrating rod [3]. In these cases, the spatial position of the liquidus and solidus are well defined and can be kept constant with regard to the ultrasonic source. Even in these technologies, however, the scaling up of the process required the use of several or more powerful ultrasonic transducers. In other casting processes where the solidification front is moving, this mechanism is not applicable at all.

One of the ways out of this impasse would be treating the melt in a fluid state, i.e. in a melt flow, targeting the fragmentation of primary intermetallics that may act as nucleation substrates for the matrix phase. Ultrasonic processing of aluminium alloys containing Zr and Ti was shown to produce a remarkable grain refining effect when applied above the liquidus of aluminium [2, 4], and the explanation lies in the refinement of primary Al_3Zr particles down to a few microns so that they become efficient nuclei for aluminium, Ti acting as a growth restriction element [44, 45].

What remained unclear is how the fragmentation of a primary phase occurs under cavitation and streaming conditions. Only *in situ* studies using synchrotron and high-speed imaging could help clarifying this. The first works in this direction showed that fracture of primary phases in metal solidification was mainly due to the shock wave (force) emitted at bubble implosion and the fatigue effect due to vigorously oscillating ultrasonic bubbles [46, 47].

We studied the fragmentation of intermetallics by cavitation bubbles in water using a high-speed camera [48]. The analysis of images revealed that the mechanism of cavitation-induced fragmentation is fatigue-like (and not instantaneous as it has been believed), with many cycles of oscillations required for an intermetallic particle to develop a crack and then break in a brittle fashion as shown in Fig. 13. The *in situ* crack growth was analysed using the literature data on the fracture toughness of intermetallics and the pressure created by either imploding or a pulsating bubble [48]. It was estimated that for the observed critical crack size of 22 μm the stress required to fracture a primary Al_3Ti crystal is between 215 and 322 MPa (at room temperature). Such a pressure can be produced upon the collapse and rebound of a cavitation bubble close to the solid interface in water [49]. A steadily pulsating bubble, however, will produce only about 10 MPa of pressure, which is not sufficient for the

fracture of the intermetallic crystal (it would require a crack size in excess of a critical value in centimetres).

For the matrix dendrites, however, in addition to the fragmentation of imploding bubbles, quasi-steady bubble oscillations may also result in the cyclic fatigue facilitated by acoustic flow (in the range of 0.5–0.6 m/s). The fatigue fracture of the Zn phase and the erosion of liquid-solid interface due to the oscillating bubbles observed in in-situ synchrotron experiments agreed very well with the theoretical calculations [31].

Acoustic flow plays an important role in fragmentation of elongated crystals and disruption of the solidification front (solid–liquid interface) as has been discovered by in-situ synchrotron observations of primary Al_2Cu in an Al-35% Cu alloy. This primary phase forms thin and elongated dendrites that look like a sea weed on a cross section, Fig. 14a. Under ultrasonic irradiation the long crystals vibrate in tune with acoustic wave and sway under recirculating acoustic streaming, with eventually separating dendrite branches that are flown away with the flow, Fig. 14b [50]. Acoustic streaming also brings a hotter melt into the semi-solid region, facilitating remelting of dendrite branches and their thinning. In this case, the stress induced by the acoustic streaming (0.5 m/s) on a thin (22 μm diameter) crystal reaches 22–24 MPa, which exceeds the yield strength of the crystal (20 MPa) [50]. The detached branches are transported by the recirculating acoustic flow upward towards the cavitation zone where they experience further fragmentation by imploding bubbles, producing small dendrite fragments that act as nuclei for the intermetallic phase in the subsequent solidification, with eventual structure refinement, Fig. 14c. This mechanism is further illustrated in Fig. 15.

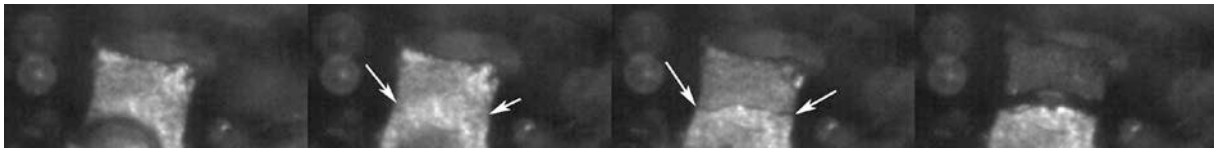

Figure 13: Images of a primary Al_3Ti crystal fragmented by a pulsating bubble (seen on the first frame). Arrows show the fatigues crack initiation and propagation. The field of view is 337.28 ×337.28 μm^2 and the images were recorded at 10^5 fps [48].

Figure 14: Fragmentation of Al_2Cu dendrites in and Al-35 wt% Cu alloy (in situ synchrotron X-ray study): (a) elongated dendrites growing without USP; (b) fragmentation (shown by arrows) of dendrites by acoustic streaming (ultrasonic source is above the left top corner); and (c) refined equiaxed crystals formed after the end of USP.

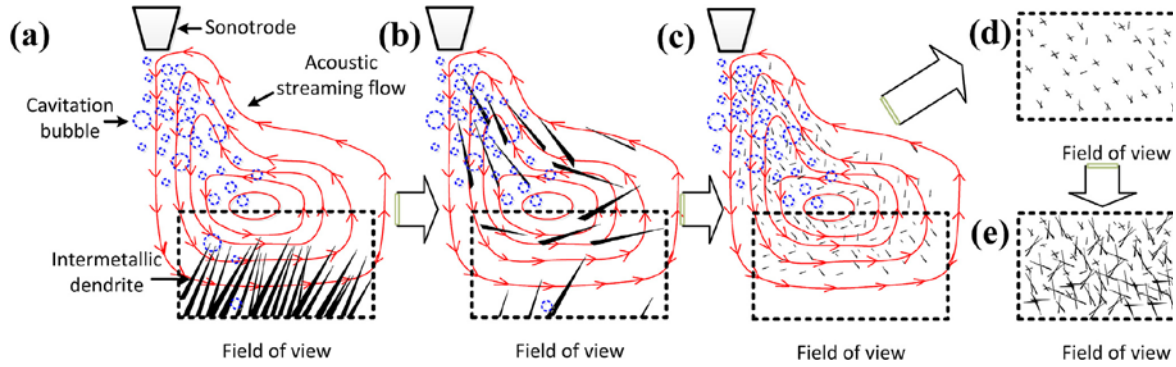

Figure 15: A schematic showing the mechanisms for microstructural refinement of primary intermetallic crystals by USP: (a) acoustic cavitation and acoustic streaming flow; (b) intermetallic dendrites are fragmented due to the combined effects of the acoustic cavitation and streaming flow (see Fig. 14b); (c) further fragmentation as the acoustic flow brings the fragments back into the cavitation zone; (d) after USP is stopped, the surviving small fragments grow as equiaxed dendrites (see Fig. 14c); (e) the equiaxed dendrites grow further leading to structure refinement.

5. De-agglomeration

Ultrasonic cavitation and acoustic streaming play a vital role in de-agglomerating and dispersing particles in liquids. With regard to liquid metal processing, these processes are important for improving the efficiency of grain refinement (de-agglomeration of TiB_2 agglomerates from commercial master alloys) [51] and manufacturing of metal-matrix composites (de-agglomeration and dispersion of reinforcing particles including nanoparticles) [34, 52]. The mechanisms of de-agglomeration were thought to include the penetration of the liquid metal into the agglomerates (overcoming capillary pressure),

followed by implosion of cavitation bubbles from inside the agglomerate, affectively dispersing the particles in the bulk. It is known, however, that dispersion of clusters, especially consisting of nanoparticles, takes a lot of time, e.g. 25–30 min for a half-kg of a Mg-based composite [53]. This is inconsistent with an explosive destruction of agglomerates from within (at least for agglomerates of a considerable size).

Recently a numerical model has been developed that describes the de-agglomeration in an ultrasonic field and demonstrates the role of particle size, acoustic pressure and liquid flow on the de-agglomeration kinetics [54]. This model does not, however, predict the processing time that is required for complete de-agglomeration.

Recent *in situ* high-speed observations of cavitation-induced de-agglomeration showed that the process actually happens from the surface of agglomerates rather than from within. Figure 16 a, b demonstrated this phenomenon for MgO clusters in water. The process more resembles chipping off individual particles from the surface rather than rupture of the agglomerate from within its bulk. This observation clearly explains why the de-agglomeration takes long time, which should be the function of the size of the agglomerates, the size of the particles, and the pressure conditions.

It can be demonstrated [35, 55] that the pressure difference Δp between the acoustic pressure from an imploding bubble close to the agglomerate and the capillary pressure inside the channel between particles is the controlling parameter for the de-agglomeration time. As these pressures are of the same order of magnitude (at least for micron-size channels), the excess pressure p_{ex} is rather small (tens of Pa), and when $p_{ex}>\Delta p$, the capillary will be filled with liquid metal after some time t_{wt}. This time can be obtained by integrating Eq. (1):

$$t_{wt} = \frac{4\eta_l {l_{cr}}^2}{R_{cr}^2 p} \tag{1}$$

With

$$\frac{l_{cr}}{R_{cr}} = \frac{8}{3} S_m D \rho_p , \tag{2}$$

where R_{cr} is the capillary channel radius, η_l is the viscosity of the melt, l_{cr} is the capillary length filled with the melt, p is the acoustic pressure, D is the average particle diameter, S_m is particles' specific surface, and ρ_p is the density of a particle. Typical values for nanoparticles from tens of nanometers to several microns in size are listed in Table 2 [56]. It is interesting that the experimental data are counterintuitive and show that particles several microns in

size may have larger specific area than nanoparticles. This is because the surface of the former is very uneven and contains a lot of folds, pores and crevices, while the surface of the latter is rather smooth.

Figure 16c shows the dependence of the time required for de-agglomeration on the l_{cr}/R_{cr} ratio for particles with the sizes from several microns to hundreds of microns. In this case the larger the particles, the lower their specific surface area and the shorter the time required for de-agglomeration. The agglomerates of small particles would require several minutes to de-agglomerate matching the experimental results (for alumina particles in aluminium: 3-5 min for 10–20 μm in diameter and 12-15 min for 0.1 to 10 in diameter [4]). In the case of nanoparticles, however, the suggested approach may not work as the capillary pressure (between the particles in a cluster) becomes so large that it outweighs the decrease in the specific surface area and may require either significantly higher pressures form cavitating bubbles (e.g. implosion pressure in aluminium is larger than in water) or much longer times for de-agglomeration (which is experienced in practice).

Table 2. Size, specific surface of powder particles (experimental, [56]) and the ratio of the length of the channels to the particle radius.

Powder	Average particle diameter	Specific surface, m^2/g	l_{cr}/R_{cr} (Eq (2))
α-Al_2O_3	36 nm	35–40	14.2
ZrO_2 (Y_2O_3)	1.5 μm	7	110
Al_2O_3	0.2–5 μm	60	465

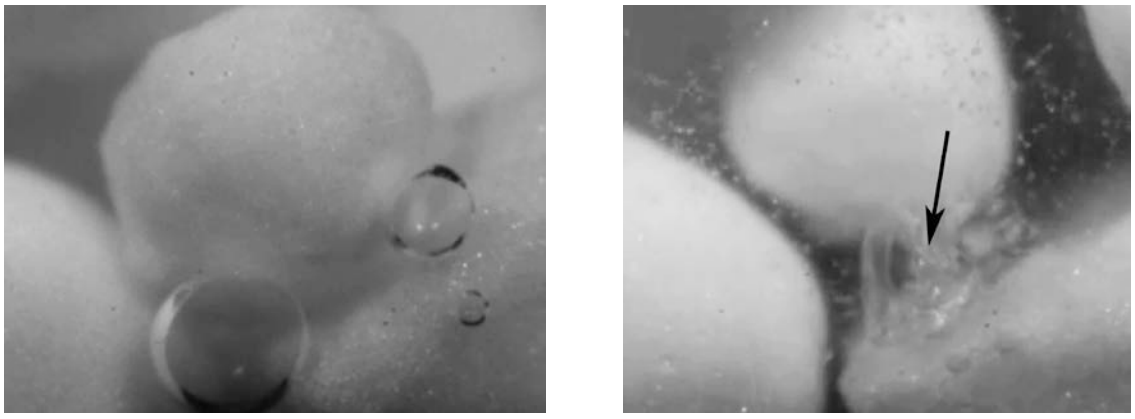

a b

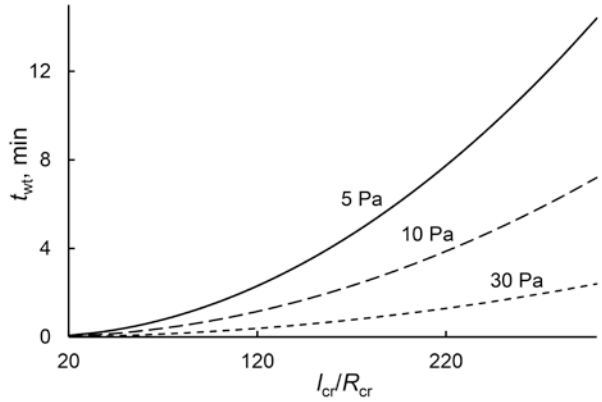

c

Figure 16: De-agglomeration: (a, b) in situ observation of de-agglomeration of MgO agglomerates by cavitation bubbles (shown by arrow) (a, stable bubbles before the onset of cavitation and b, imploding and rebounding bubbles producing de-agglomeration); (c) dependence of the penetration time of melt into the channels between the particles on the ratio of length to radius of the channel for various values of the differential pressure Δp (after [35]).

6. Conclusion

Application of modern characterisation techniques allows researchers to get an insight into the mechanisms of ultrasonic melt processing, both from physical and mechanical points of view. These insights are invaluable for establishing reliable models of USP and upscaling USP to various industrial applications.

In the last 5 years we carried out extensive experimental and numerical studies, and this work established that:

- Acoustic shielding plays a very important role in the propagation of sound waves and active cavitation throughout the volume of a treated liquid.

-The acoustic pressure in the treated volume, outside the cavitation zone, can be higher at a lower driving power of the transducer, which is very important for practical applications.

-Although water can be used as a suitable transparent analogue of liquid aluminium for qualitative studies of ultrasonic processing, the acoustic pressure, both in a driving-frequency and in the MHz range of acoustic spectrum, is much higher in liquid aluminium.

-Acoustic streaming induced by a sonotrode can have different direction (towards, or away from its surface) depending on the cavitation intensity and the amount of bubbles in the cavitation zone.

-The sonocapillary effect observed for the first time in liquid aluminium plays an important role in de-agglomerating particles clusters.

-Ultrasonic de-agglomeration is a gradual process occurring from the surface of an agglomerate and enforced by oscillating and imploding bubbles.

-Ultrasonic cavitation facilitates the nucleation of primary crystals on oxides in liquid metals.

-Fragmentation of solid crystals in cavitating liquids occurs through a fatigue-like mechanism triggered by oscillating bubbles and alternating acoustic flows.

-Quantified experimental observations of cavitation-related phenomena supplemented by acoustic measurements give invaluable input to numerical modelling as well as provided validation of the models.

Acknowledgements

Authors gratefully acknowledge the support from EPSRC grants (EP/K005804/1, EP/K00588X/1, EP/I02249X/1, EP/L019884/1, EP/L019825/1, EP/L019965/1, EP/R011001/1, EP/R011095/1 and EP/R011044/1) and EU FP7 grants (286344, 606090, NMP3-LA-2012–280421). J. Mi would like also to acknowledge the financial support of the Royal Society Industry Fellowship in 2012–2016; and the awards of synchrotron X-ray beam time EE8542-1 and NT12131-1 by the Diamond Light Source, UK; No. 20160076 by the Synchrotron SOLEIL, France; and GUP 23649 and GUP 26170 by the Advanced Photon Source, Argonne National Laboratory, USA. Use of the Advanced Photon Source, an Office of Science User Facility operated for the U.S. Department of Energy (DOE) Office of Science by Argonne National Laboratory, was supported by the U.S. DOE under Contract No. DE-AC02-06CH11357.

We would like also to thank Prof. P.D. Lee, Dr W. Mirihanage, Dr W.W. Xu, Dr V.M. Sreekumar and Dr O.B. Kudryashova for their valuable contribution to the presented results.

References

1. G.I Eskin, Ultrasonic Treatment of Molten Aluminium, Metallurgiya, Moscow, 1965.

2. G.I Eskin, Ultrasonic Treatment of Molten Aluminium, Second Edn., Metallurgiya, Moscow, 1988.

3. O.V. Abramov, Crystallisation of Metals in Ultrasonic Field, Metallurgiya, Moscow, 1972.

4. G.I. Eskin, D.G. Eskin, Ultrasonic Treatment of Light Alloys Melts, Second Edn., CRC Press, Boca Raton, 2015.

5. L. Rozenberg (Ed.), High Intensity Ultrasonic Fields. Nauka, Moscow, 1968.

6. V.I. Il'ichev, Cavitation strength of liquids and onset of cavitation, Proc. Acust. Inst. Acad. Sci. USSR. 6 (1969) 16-29.

7. O.A. Kapustina, in: Physical Principles of Ultrasonic Technology, Nauka, Moscow, 1970, pp. 253-336.

8. E.G. Konovalov, I.N. Germanovich, Ultrasonic capillary effect, Dokl. Akad. Nauk. Belorus. 6 (1962) 492-493.

9. P.P. Prokhorenko, N.V. Dezhkunov, G.E. Konovalov, Ultrasonic Capillary Effect, Nauka i Tekhnika, Minsk, 1981.

10. G.M. Swallowe, J.E. Fields, C.S. Rees, A. Duckworth, A photographic study of the effect of ultrasound on solidification, Acta. Metall. 37 (1989) 961-967.

11. I. Tudela, V. Sáez, M.D. Esclapez, M.I. Díez-García, P. Bonete, J. González-García, Simulation of the spatial distribution of the acoustic pressure in sonochemical reactors with numerical methods: A review, Ultrason. Sonochem. 21 (2014) 909–919. doi:10.1016/j.ultsonch.2013.11.012.

12. O. Louisnard, A simple model of ultrasound propagation in a cavitating liquid. Part I: Theory, nonlinear attenuation and traveling wave generation, Ultrason. Sonochem. 19 (2012) 56–65. doi:10.1016/j.ultsonch.2011.06.007.

13. H. Dogan, V. Popov, Numerical simulation of the nonlinear ultrasonic pressure wave propagation in a cavitating bubbly liquid inside a sonochemical reactor, Ultrason. Sonochem. 30 (2016) 87–97. doi:10.1016/j.ultsonch.2015.11.011.

14. F.J. Trujillo, A strict formulation of a nonlinear Helmholtz equation for the propagation of sound in bubbly liquids. Part I: Theory and validation at low acoustic pressure amplitudes, Ultrason. Sonochem. 47 (2018) 75–98. doi:10.1016/j.ultsonch.2018.04.014.
15. O. Louisnard, A viable method to predict acoustic streaming in presence of cavitation, Ultrason. Sonochem. 35 (2017) 518–524. doi:10.1016/j.ultsonch.2016.09.013.
16. I. Tzanakis, M. Hodnett, G.S.B. Lebon, N. Dezhkunov, D.G. Eskin, Calibration and performance assessment of an innovative high-temperature cavitometer, Sens. Actuators Phys. 240 (2016) 57–69, http://dx.doi.org/10.1016/j.sna.2016.01.024.
17. I. Tzanakis, G.S.B. Lebon, D.G. Eskin, K.A. Pericleous, Characterisation of the ultrasonic acoustic spectrum and pressure field in aluminium melt with an advanced cavitometer, J. Mater. Process. Technol. 229 (2016) 582–586, http://dx.doi.org/10.1016/j.jmatprotec.2015.10.009.
18. I. Tzanakis, G.S.B. Lebon, D.G. Eskin, K.A. Pericleous, Characterizing the cavitation development and acoustic spectrum in various liquids, Ultrason. Sonochem. 34 (2017) 651–662, http://dx.doi.org/10.1016/j.ultsonch.2016.06.034.
19. W.W. Xu, I. Tzanakis, P. Srirangam, W.U. Mirihanage, D.G. Eskin, A.J. Bodey, P.D. Lee, Synchrotron quantification of ultrasound cavitation and bubble dynamics in Al–10Cu melts, Ultrason. Sonochem. 31 (2016) 355–361, http://dx.doi.org/10.1016/j.ultsonch.2016.01.017.
20. I. Tzanakis, W.W. Xu, D.G. Eskin, P.D. Lee, N. Kotsovinos, In situ observation and analysis of ultrasonic capillary effect in molten aluminium, Ultrason. Sonochem. 27 (2015) 72–80, http://dx.doi.org/10.1016/j.ultsonch.2015.04.029.
21. I. Tzanakis, G.S.B. Lebon, D.G. Eskin, K.A. Pericleous, Investigation of the factors influencing cavitation intensity during the ultrasonic treatment of molten aluminium, Mater. Design, 90 (2016) 979–983 https://doi.org/10.1016/j.matdes.2015.11.010.
22. D.G. Eskin, K. Al-Helal, I. Tzanakis, Application of a plate sonotrode to ultrasonic degassing of aluminum melt: Acoustic measurements and feasibility study, J. Mater. Process. Technol. 222 (2015) 148–154. http://dx.doi.org/10.1016/j.jmatprotec.2015.03.006.
23. L.V. Wijngaarden, On the equations of motion for mixtures of liquid and gas bubbles, J. Fluid Mech. 33 (1968) 465–474. doi:10.1017/S002211206800145X.
24. R.E. Caflisch, M.J. Miksis, G.C. Papanicolaou, L. Ting, Effective equations for wave propagation in bubbly liquids, J. Fluid Mech. 153 (1985) 259–273. doi:10.1017/S0022112085001252.

25. L.L. Foldy, The Multiple Scattering of Waves. I. General Theory of Isotropic Scattering by Randomly Distributed Scatterers, Phys. Rev. 67 (1945) 107–119. doi:10.1103/PhysRev.67.107.
26. G.S.B. Lebon, K. Pericleous, I. Tzanakis, D.G. Eskin, Dynamics of two interacting hydrogen bubbles in liquid aluminum under the influence of a strong acoustic field, Phys. Rev. E. 92 (2015) 043004. doi:10.1103/PhysRevE.92.043004.
27. A. Doinikov, Translational motion of two interacting bubbles in a strong acoustic field, Phys. Rev. E. 64 (2001) 026301. doi:10.1103/PhysRevE.64.026301.
28. G.S.B. Lebon, I. Tzanakis, G. Djambazov, K. Pericleous, D.G. Eskin, Numerical modelling of ultrasonic waves in a bubbly Newtonian liquid using a high-order acoustic cavitation model, Ultrason. Sonochem. 37 (2017) 660–668. http://dx.doi.org/10.1016/j.ultsonch.2017.02.031.
29. H. Huang, D. Shu, Y. Fu, J. Wang, B. Sun. Synchrotron radiation X-ray imaging of cavitation bubbles in Al–Cu alloy melt, Ultrason. Sonochem. 21 (2014) 1275–1278. http://dx.doi.org/10.1016/j.ultsonch.2013.12.024
30. D. Tan, T.L. Lee, J.C. Khong, T. Connolley, K. Fezzaa, J. Mi. High-speed synchrotron X-ray imaging studies of the ultrasound shockwave and enhanced flow during metal solidification processes, Metall. Mater. Trans. A, 46A (2015) 2851–2861. https://doi.org/10.1007/s11661-015-2872-x
31. B. Wang, D. Tan, T.L. Lee, J.C. Khong, F. Wang, D. Eskin, T. Connolley, K. Fezzaa, J. Mi, Ultrafast synchrotron X-ray imaging studies of microstructure fragmentation in solidification under ultrasound, Acta Mater. 144 (2018) 505–515. doi.org/10.1016/j.actamat.2017.10.067
32. M. Minnaert, XVI. On musical air-bubbles and the sounds of running water, Lond. Edinb. Dublin Philos. Mag. J. Sci. 16 (1933) 235–248. doi:10.1080/14786443309462277.
33. H. Choi, M. Jones, H. Konishi, Effect of Combined Addition of Cu and Aluminum Oxide Nanoparticles on Mechanical Properties and Microstructure of Al-7Si-0.3Mg Alloy, Metall. Mater. Trans. A, 43A (2012) 738–746. https://doi.org/10.1007/s11661-011-0905-7
34. S.A. Vorozhtsov, D.G. Eskin, J. Tamayo, A.B. Vorozhtsov, V.V. Promakhov, A.A. Averin, A.P. Khrustalyev, The application of external fields to the manufacturing of novel dense composite master alloys and aluminum-based nanocomposites, Metall. Mater. Trans. A, 46A (2015) 2870–2875. DOI: 10.1007/s11661-015-2850-3

35. O. Kudryashova, S. Vorozhtsov, On the mechanism of ultrasound-driven de-agglomeration of nanoparticle agglomerates in aluminum melt, JOM. 68 (2016) 1307–1311. DOI: 10.1007/s11837-016-1851-z

36. W. Mirihanage, W. Xu, J. Tamayo-Ariztondo, D. Eskin, M. Garcia-Fernandez, P. Srirangam, P.D. Lee, Synchrotron radiographic studies of ultrasonic melt processing of metal matrix nano composites, Mater. Lett. 164 (2016) 484–487. https://doi.org/10.1016/j.matlet.2015.11.022

37. M.C. Schenker, M.J.B.M Pourquie, D.G. Eskin, B.J. Boersma, PIV quantification and numerical modelling of the flow induced by an ultrasonic horn, Ultrason. Sonochem. 20 (2013) 502–509. https://doi.org/10.1016/j.ultsonch.2012.04.014

38. O.V. Abramov, I.I. Teumin, Crystallization of Metals. In: Physical Principles of Ultrasonic Technology, ed. L.D. Rozenberg, Nauka, Moscow, 1970, pp. 427–514.

39. F. Wang, D. Eskin, T. Connolley, C. Wang, B. Koe, A. King, C. Reinhard, J. Mi, In-situ synchrotron X-ray radiography observation of primary Al_2Cu intermetallic growth on fragments of aluminium oxide film, Mater. Lett. 213 (2018) 303–305. DOI: 10.1016/j.matlet.2017.11.090

40. F. Wang, D. Eskin, J. Mi, T. Connolley, M. Mounib, J. Lindsay. A refining mechanism of primary Al_3Ti intermetallic particles by ultrasonic treatment in the liquid state, Acta Materilaia 116 (2016) 354–363. doi:10.1016/j.actamat.2016.06.056

41. F. Wang, D. Eskin, T. Connolley, J. Mi, Influence of ultrasonic treatment on the formation of primary Al_3Zr in an Al-0.4 Zr alloy, Trans. Nonferr. Met. Soc. China, 2017, vol. 27, pp. 977−985. DOI: 10.1016/S1003-6326(17)60115-8

42. V.M. Sreekumar, N. Hari Babu, D.G Eskin, Prospects of In-Situ α-Al_2O_3 as an inoculant in aluminum: A Feasibility Study, J. Mater. Eng. Perform. 26 (2017) 4166–4176. DOI: 10.1007/s11665-017-2853-x

43. V.M. Sreekumar, N. Hari Babu, D.G. Eskin, Potential of Al-Ti-$MgAl_2O_4$ master alloy and ultrasonic cavitation on the grain refinement of a cast aluminum alloy, Metall. Mater. Trans. B 48B (2017) 208–219. DOI: 10.1007/s11663-016-0824-5

44. T.V. Atamanenko, D.G. Eskin, L. Zhang, L. Katgerman, Criteria of grain refinement induced by ultrasonic melt treatment of aluminum alloys containing Zr and Ti, Metall. Mater. Trans. A 41A (2010) 2056–2066. https://doi.org/10.1007/s11661-010-0232-4

45. T.V. Atamanenko, D.G. Eskin, M. Sluiter, L. Katgerman, On the mechanism of grain refinement in Al–Zr–Ti alloys, J. Alloys Comp. 509 (2011) 57–60. doi.org/10.1016/j.jallcom.2010.09.046

46. D. Shu, B. Sun, J. Mi, P. S. Grant, A High-Speed Imaging and Modeling Study of Dendrite Fragmentation Caused by Ultrasonic Cavitation, Metall. Mater. Trans. A 44A (2012) 3755–3766. doi.org/10.1007/s11661-012-1188-3

47. J. Mi, D. Tan, T. L. Lee, In situ synchrotron X-ray study of ultrasound cavitation and its effect on solidification microstructures, Metall. Mater. Trans. B 46B (2015) 1615–1619. doi.org/10.1007/s11663-014-0256-z

48. F. Wang, I. Tzanakis, D. Eskin, T. Connolley, J. Mi, In-situ observation of ultrasonic cavitation-induced fragmentation of the primary crystals formed in Al alloys, Ultrason. Sonochem. 39 (2017) 66–76. DOI 10.1016/j.ultsonch.2017.03.057

49. G.S.B. Lebon, A. Kao, K. Pericleous, The uncertain effect of cavitating bubbles on dendrites, in: Proc. 6th Decenn. Int. Conf. Solidif. Process., Old Windsor, UK, 2017: pp. 554–557.

50. Wang F, Eskin D, Mi J, Wang C, Koe B, King A, Reinhard C, Connolley T. A synchrotron X-radiography study of the fragmentation and refinement of primary intermetallic particles in an Al-35Cu alloy induced by ultrasonic melt processing, Acta Mater., 2017, vol. 141, pp. 142–153.

51. G.I. Eskin, A.A. Rukhman, S.G Bochvar, V.Ya. Elfimov and D.V. Konovalov. New developments in the technology of ultrasonic melt treatment if light alloys, Tsvetn. Met. (3) (2008) 105–110.

52. G.I. Eskin, D.G. Eskin. Production of natural and synthesized aluminum-based composite materials with the aid of ultrasonic (cavitation) treatment of the melt, Ultrason. Sonochem. 10 (2003) 297–301. doi:10.1016/S1350-4177(02)00158-X

53. G. Cao, H. Konishi, X. Li. Mechanical properties and microstructure of SiC-reinforced Mg-(2,4)Al-1Si nanocomposites fabricated by ultrasonic cavitation based solidification processing, Mater. Sci. Eng. A. 486 (2008) 357–362. doi: 10.1016/j.msea.2007.09.054

54. A. Manoylov, B. Lebon, G. Djambazov, K. Pericleous. Coupling of acoustic cavitation with Dem-based particle solvers for modeling de-agglomeration of particle clusters in liquid metals, Metall. Mater. Trans. A. 48A (2017) 5616–5627. DOI: 10.1007/s11661-017-4321-5

55. O.B. Kudryashova, D.G. Eskin, A.P. Khrustalev, S.A.Vorozhtsov. Ultrasonic effect on the penetration of the metallic melt into submicron particles and their agglomerates, Russian Journal of Non-Ferrous Metals, 58 (2017) 427–433.
https://doi.org/10.3103/S1067821217040101
56. S. Vorozhtsov, I. Zhukov, A. Vorozhtsov, A. Zhukov, D. Eskin, A. Kvetinskaya, Synthesis of micro- and nanoparticles of metal oxides and their application for reinforcement of Al-based alloys, Adv. Mater. Sci. Eng. 2015 (2015) 718207 http://dx.doi.org/10.1155/2015/718207

Figure captions

Figure 1: Experimental measurements of acoustic emissions and pressure: (a) acoustic spectra acquired under the sonotrode in water (lower curve and liquid aluminium (upper curve) and distribution of average acoustic pressure with a distance from the sonotrode in the same volume (2 l) of water (b) and liquid aluminium (c). See Table 1 for the acoustic power in W corresponding to the transducer power in %.

Figure 2: Variation of maximum pressure with distance from sonotrode [28] and comparison with experimental cavitation intensity [21].

Figure 3: (a) An X-ray image sequence acquired using 135,780 fps at Sector 32-ID-B of APS, showing the bubble implosion immediately below the sonotrode tip in a Bi–8% Zn alloy. (b) The bubble radius evolution and correlation with the acoustic pressure applied into the liquid metal (adapted from [31]).

Figure 4: The transient behaviour of a cavitation bubble in an Al–10 wt% Cu melt (640 °C, 30 kHz, 800 W/cm^2) captured by synchrotron X-rays.

Figure 5: Experimentally measured bubble size distribution (a) and growth kinetics (b) of stable cavitation bubbles in an Al-10 wt% Cu melt (640 °C, 30 kHz, 800 W/cm^2) (after [19]).

Figure 6: Acoustic streaming and dendrite fragmentation (arrows) observed in a synchrotron using a Sn–30 wt% Cu alloy and 100 W acoustic power.

Figure 7: Synchrotron X-ray observation of flow patterns and cavitation bubble population in an Al–10 wt% Cu alloys (a, b) and an Al–10 wt% Cu alloy with 0.05 wt% of 80-nm Al_2O_3 particles (c, d) (700 °C, 30 kHz, 800 W/cm^2) [36]. (a, c)–during USP, (b, d)–immediately after USP has been stopped.

Figure 8: The development of the cavitation zone and acoustic flow patterns in three transparent liquids: water (upper row), ethanol (middle row) and glycerine (lower row) (RT, 20 kHz, acoustic power 90, 78 and 230 W at the same oscillation amplitude 17 µm p-p) (after [18]).

Figure 9: Typical average velocity fields (a, b) and stream lines (c, d) measured with PIV below the sonotrode tip at a low (a, c) and high (b, d) transducer power settings. The axial direction of streaming is upwards in (a, c) and downwards in (b, d). Legend: velocity magnitude in m/s (0.01–0.1 left, 0.04–0.6 right).

Figure 10: Refinement of primary Al_3Zr particles in an Al–0.4 wt% Zr alloy: (a) without USP; (b) after USP performed above the liquidus of Al_3Zr and (c) nucleating oxide inclusion inside an Al_3Zr particle.

Figure 11: In-situ synchrotron observation of the nucleation of primary Al_2Cu crystals (dark) on the fragments of alumina film (bright) in an Al-35 wt% Cu alloy. Temperature decreases from left to right.

Figure 12: Effect of oxides and USP on the grain refining in an A357 (Al-Si-Mg) aluminium alloy: a, A357 cast with USP, no grain refiner; b, A357 cast with an addition of 1% alumina-containing master alloy; c, same as (b) but with USP; d, effects of spinel-containing master alloy addition and USP on the grain size in an A357 alloy.

Figure 13: Images of a primary Al_3Ti crystal fragmented by a pulsating bubble (seen on the first frame). Arrows show the fatigues crack initiation and propagation. The field of view is 337.28 ×337.28 μm^2 and the images were recorded at 10^5 fps [48].

Figure 14: Fragmentation of Al_2Cu dendrites in and Al-35 wt% Cu alloy (in situ synchrotron X-ray study): (a) elongated dendrites growing without USP; (b) fragmentation (shown by arrows) of dendrites by acoustic streaming (ultrasonic source is above the left top corner); and (c) refined equiaxed crystals formed after the end of USP.

Figure 15: A schematic showing the mechanisms for microstructural refinement of primary intermetallic crystals by USP: (a) acoustic cavitation and acoustic streaming flow; (b) intermetallic dendrites are fragmented due to the combined effects of the acoustic cavitation and streaming flow (see Fig. 14b); (c) further fragmentation as the acoustic flow brings the fragments back into the cavitation zone; (d) after USP is stopped, the surviving small fragments grow as equiaxed dendrites (see Fig. 14c); (e) the equiaxed dendrites grow further leading to structure refinement.

Figure 16: De-agglomeration: (a, b) in situ observation of de-agglomeration of MgO agglomerates by cavitation bubbles (shown by arrow) (a, stable bubbles before the onset of

cavitation and b, imploding and rebounding bubbles producing de-agglomeration); (c) dependence of the penetration time of melt into the channels between the particles on the ratio of length to radius of the channel for various values of the differential pressure Δp (after [35]).